THE GLOBAL PHASE SPACE OF THE THREE-VORTEX INTERACTION SYSTEM

A. ANURAG AND R. H. GOODMAN

ABSTRACT. We derive a symplectic reduction of the evolution equations for a system of three point vortices and use the reduced system to succinctly explain a kind of bifurcation diagram that has appeared in the literature in a form that was difficult to understand and interpret. Using this diagram, we enumerate and plot all the global phase-space diagrams that occur as the circulations of the three vortices are varied. The reduction proceeds in two steps: a reduction to Jacobi coordinates and a Lie-Poisson reduction. In a recent paper, we used a different method in the second step. This took two forms depending on a sign that arose in the calculation. The Lie-Poisson equations unify these into a single form. The Jacobi coordinate reduction fails when the total circulation vanishes. We adapt the reduction method to this case and show how it relates to the non-vanishing case.

1. INTRODUCTION

The motion of N vortices is a significant problem in the history of dynamical systems and fluid mechanics, dating back to its derivation by Helmholtz and its Hamiltonian formulation by Kirchhoff [18, 33]. Gröbli made the first systematic study of solutions to this system in his 1877 doctoral thesis [13].

The system dynamics are trivial for $N = 1$ and $N = 2$, while the simplest nontrivial case occurs for $N = 3$. Gröbli formally reduced this system to quadratures, predating Poincaré's introduction of the dynamical systems approach to systems of ordinary differential equations, so it does not include phase-plane analysis in the modern sense. The reduced equations form a closed system describing the evolution of the three pairwise distances between the particles. This system, which has been rediscovered several times [2, 25], introduces a singularity into the coordinate system at all collinear arrangements of the vortices. Such arrangements occur frequently, complicating the use of these coordinates to understand the dynamics.

Since Gröbli, many different coordinate systems have been derived to describe the dynamics. Finding the right one can reveal features in the dynamics that are otherwise difficult or impossible to see. Synge interpreted Gröbli's coordinates as describing trilinear coordinates for the plane, allowing him to apply phase-plane reasoning, an approach rediscovered by Aref [2, 31]. The singularity at collinear configurations becomes a singular curve in the phase plane. To overcome this difficulty, many groups have derived coordinate systems to describe particular phenomena, such as scattering or self-similar collapse, but none apply globally [7, 8, 10, 11, 19, 21, 30–32].

In our previous paper [1], we reduced the motion of three vortices to a simple form in three steps. In the first step, we used Jacobi coordinates to mod out the system's translation invariance. In the second step, we normalized the variables to eliminate the dependence of the Poisson bracket on the vortices' circulations. We further reduced the system using the Nambu bracket formulation in the third step. The normalization step depends on the sign σ of a parameter κ_2 that arises in the reduction, and the final system of equations takes different forms depending on σ.

In this paper, we describe a near-universal reduced system of equations that encompasses both forms of the final system. We follow a Jacobi coordinate reduction with a Lie-Poisson reduction. This method eliminates the need for the normalization step used in our previous paper and unifies the two final forms of the system into a single system of equations. The reduced equations describe the shape-space evolution of the vortex three-body problem as Montgomery did for the gravitational three-body problem, for example, in [23]. Because the circulation of a vortex is a signed quantity, the shape space may be spherical, as in the

Date: April 22, 2025.

gravitational problem, or unbounded. We use this to explain all the bifurcations in the three-vortex system as the circulations vary. The second reduction step follows a procedure outlined by Ohsawa [26–28], but that work uses a different reduction at the first step. Jacobi coordinates have been applied to the three-vortex problem, notably in Refs. [15, 21]. Hernández-Garduño derived a Lie-Poisson form of the equations by a different route in Ref. [14].

The reduction applies in all cases except when the total circulation of the three vortices vanishes, in which case it becomes singular. Although an effective reduction method is well known [3, 29], we include a version here for completeness, which hews closely to the method we describe for nonvanishing total circulation. These two reductions suffice to describe all possible phenomena in three-vortex dynamics.

The methods operate on the Hamiltonian, simplifying its derivation and use compared to many previous reductions operating on the system of evolution equations. The transformation to Jacobi coordinates is straightforward: It is a linear transformation that involves only two variables at a time and is implemented iteratively. The second transformation is simple algebraically. Understanding its motivation requires some knowledge of the modern geometric approach to Hamiltonian mechanics, but the algebra needed to use it is, in fact, more straightforward than most of the approaches referenced above.

We use the reduced equations to enumerate all the *relative equilibria* of the three-vortex problem, their stability, and the parameter values at which they bifurcate. This has been addressed before, notably in Conte's 1979 Thése d'État, a 1988 paper by Tavantzis and Ting, and a 2009 paper by Aref [4, 10, 11, 32]. The first and last contain a high-level bifurcation diagram, which we recreate here. The new coordinates allow us to explain it more straightforwardly than previous authors.

This paper is organized as follows. In Sec. 2, we introduce the point-vortex model and some of the Hamiltonian mechanics machinery used to study it. We apply reduction methods to arrive at the final form of the equations for nonvanishing total circulation. Sec. 3 analyzes the reduced equations to describe the fixed points and their stability. This section uses discriminants and resultants computed using Mathematica to find curves in parameter space where bifurcations occur, summarized in Fig. 3.1. In Sec. 4, we plot the phase portrait for the dynamics at different points in the parameter space described by the figure. We concentrate on the case when two vortices have equal circulation. This condition simplifies the equations sufficiently to find all the equilibria in closed form and introduces additional symmetry into the phase portraits. The above sections consider only the case of nonvanishing total circulation. When this vanishes, the Jacobi coordinate reduction cannot be completed. In Sec. 5, we describe a change of variables that works in its place. We use it to derive a reduced form of the evolution equations and discuss the resulting dynamics. We conclude in Sec. 6 and discuss other problems where our analysis should apply. The paper includes two short appendices. In Sec. A, we discuss the resultant and the discriminant, two functions that allow us to understand how the number and stability of the equilibria vary with the changing circulations. Sec. B describes the trilinear coordinates used to construct Fig. 3.1.

2. The point-vortex model and Hamiltonian background

We consider a system of N vortices with positions represented in the complex form $z_j = x_j + \mathrm{i}y_j$ and nonzero circulations $2\pi\Gamma_j$. These move according to

$$\dot{x}_j = -\sum_{\substack{i=1\\ i\neq j}}^{N} \frac{\Gamma_i (y_j - y_i)}{\left|z_j - z_i\right|^2}, \quad \dot{y}_j = \sum_{\substack{i=1\\ i\neq j}}^{N} \frac{\Gamma_i (x_j - x_i)}{\left|z_j - z_i\right|^2}. \tag{2.1}$$

This can be written as a Hamiltonian system of equations

$$\frac{\mathrm{d}x_j}{\mathrm{d}t} = \frac{1}{\Gamma_j}\frac{\partial H}{\partial y_j}, \quad \frac{\mathrm{d}y_j}{\mathrm{d}t} = \frac{-1}{\Gamma_j}\frac{\partial H}{\partial x_j}, \tag{2.2}$$

where

$$H(\mathbf{z}) = \frac{-1}{2}\sum_{i<j}^{N} \Gamma_j \Gamma_j \log\left|z_i - z_j\right|^2. \tag{2.3}$$

Using the complex form directly, we may rewrite this as

$$\dot{z}_j = \mathrm{i}\sum_{\substack{i=1\\ i\neq j}}^{N} \frac{\Gamma_i(z_j - z_i)}{\left|z_j - z_i\right|^2} = \frac{-2\mathrm{i}}{\Gamma_j}\frac{\partial H}{\partial z_j^*}, \tag{2.4}$$

where the superscript asterisk denotes complex conjugation.

Helmholtz first derived the equations of motion, and Kirchhoff put them in Hamiltonian form [18, 33]. The system is a standard topic in elementary courses in mathematical fluid mechanics [9]. Newton's textbook point vortex dynamics contains a wealth of information on the subject [24].

We give a brief overview of the Hamiltonian formulation of this system based on the presentation in [27, 28]; see those references for a more complete description. It is convenient to arrange the vortex positions into a vector $\mathbf{r} = (x_1, \ldots, x_N, y_1, \ldots, y_N) \in \mathbb{R}^{2N}$ and to identify this with a vector $\mathbf{z} \in \mathbb{C}^N$. The $N \times N$ matrix

$$\mathsf{D}_\Gamma := \mathrm{diag}(\Gamma_1, \ldots, \Gamma_N) \tag{2.5}$$

and the $(2N) \times (2N)$ matrix

$$\mathbb{J} := \begin{bmatrix} 0 & \mathsf{D}_\Gamma \\ -\mathsf{D}_\Gamma & 0 \end{bmatrix} \tag{2.6}$$

defines a symplectic form on $\mathbb{R}^{2N}$. The function $H(\mathbf{z})$ defines a Hamiltonian vector field X_H on $\mathbb{R}^{2N} \cong \mathbb{C}^N$ by

$$X_H(\mathbf{z}) := \left(\mathbb{J}^{\mathsf{T}}\right)^{-1} DH(\mathbf{z}) = -\mathbb{J}^{-1} DH(\mathbf{z}), \tag{2.7}$$

where

$$\left(\mathbb{J}^{\mathsf{T}}\right)^{-1} = -\mathbb{J}^{-1} = \begin{bmatrix} 0 & \mathsf{D}_\Gamma^{-1} \\ -\mathsf{D}_\Gamma^{-1} & 0 \end{bmatrix} \tag{2.8}$$

and $\mathsf{D}_\Gamma = \mathrm{diag}\left(\Gamma_1^{-1}, \ldots, \Gamma_N^{-1}\right)$.

This allows us to define a circulation-dependent Poisson bracket of two C^1 functions from $\mathbb{C}^N$ to $\mathbb{C}$:

$$\begin{aligned} \{F(\mathbf{z}), G(\mathbf{z})\} &= X_F(\mathbf{z})^{\mathsf{T}} \mathbb{J} X_G(\mathbf{z}) \\ &= DF(\mathbf{z})^{\mathsf{T}} \left(\mathbb{J}^{\mathsf{T}}\right)^{-1} DG(\mathbf{z}) \\ &= \sum_{j=1}^{N} \frac{1}{\Gamma_j}\left(\frac{\partial F}{\partial x_j}\frac{\partial G}{\partial y_j} - \frac{\partial F}{\partial y_j}\frac{\partial G}{\partial x_j}\right). \end{aligned} \tag{2.9}$$

One consequence of the Poisson bracket formulation is that, using system (2.2), any function $F(\mathbf{z})$ evolves according to

$$\frac{\mathrm{d}}{\mathrm{d}t} F(\mathbf{z}) = X_H(F) \equiv \{F(\mathbf{z}), H(\mathbf{z})\}, \tag{2.10}$$

and, in particular

$$\frac{\mathrm{d}\mathbf{z}}{\mathrm{d}t} = X_H(\mathbf{z}) \equiv \{\mathbf{z}, H(\mathbf{z})\}. \tag{2.11}$$

This system conserves the quantities

$$\mathbf{M} = M_x + \mathrm{i}M_y = \sum_{j=1}^{N} \Gamma_j z_j, \quad \text{and} \quad \Theta = \sum_{j=1}^{N} \Gamma_j \left|z_j\right|^2. \tag{2.12}$$

The quantity $\mathbf{M}$ is the *linear impulse*, and Θ, the *angular impulse*. In the case that $\gamma_1 = \sum_{j=1}^{N} \Gamma_j \neq 0$, then

$$z_0 = \mathbf{M}/\gamma_1 \tag{2.13}$$

defines the conserved center of vorticity. The expression γ_1 is the degree-one *symmetric polynomial* in N variables, so called due to its invariance under permutations of the vortex labels. For later reference, we define the three symmetric polynomials in three circulations,

$$\gamma_1 = \Gamma_1 + \Gamma_2 + \Gamma_3, \quad \gamma_2 = \Gamma_1\Gamma_2 + \Gamma_3\Gamma_1 + \Gamma_2\Gamma_3, \quad \text{and} \quad \gamma_3 = \Gamma_1\Gamma_2\Gamma_3. \tag{2.14}$$

Any symmetric polynomial of degree greater than 3 (or, more generally, whose degree exceeds the number of independent variables) can be written as a polynomial in the γ_j.

The conservation laws arise due to the system's invariance under orientation-preserving rigid transformations, or more specifically, the system has $\mathsf{SE}(2) = \mathsf{SO}(2) \ltimes \mathbb{R}^2$ symmetry under the action

$$\mathsf{SE}(2) \times \mathbb{C}^N \to \mathbb{C}^N;\ \left(\left(e^{\mathrm{i}\psi}, a\right), \mathbf{z}\right) \mapsto e^{\mathrm{i}\psi}\mathbf{z} + a\mathbf{1}, \tag{2.15}$$

where $\mathbf{1} = (1, \ldots, 1)^{\mathsf{T}}$. Here, $\mathsf{SE}(2)$ is the special Euclidean group of orientation-preserving rigid deformations of the plane. All such deformations can be written as the composition of a rotation $e^{\mathrm{i}\psi} \in \mathsf{SO}(2)$ followed by a translation by $a \in \mathbb{R}^2$. The "$\ltimes$" symbol denotes that $\mathsf{SE}(2)$ is the semidirect product of the rotation and translation groups in the plane.

The two changes of variables described below reduce the dimension of the system. The first, a Jacobi coordinate reduction, removes the translations by $a\mathbf{1}$. The second, which puts the equations in Lie-Poisson form, eliminates the rotations by $e^{\mathrm{i}\psi}$. *Canonical* changes of variables, i.e., those that preserve the system's Hamiltonian structure, are preferable, as they allow us to work with the scalar-valued Hamiltonian function rather than the ODE system. Doing this without introducing new singularities will require a more general definition of Hamiltonian mechanics than has been common in the point-vortex literature.

2.1. **Jacobi Coordinate Reduction.** The Jacobi coordinate reduction is a canonical change of variables that allows us to systematically introduce the center of vorticity z_0, defined in (2.13), as a variable. Because z_0 does not vary, this procedure reduces the number of degrees of freedom by one. In addition to constructing a change of the coordinates z_j, the procedure changes the form of the Poisson bracket (2.9) by introducing new circulation variables $\tilde{\Gamma}_j$. It proceeds iteratively, replacing two conjugate pairs of variables at a time, repeating the procedure $N-1$ times until all the variables have been replaced, so when $N = 3$, it takes two steps.

Consider a Hamiltonian system of the form (2.3) with $\Gamma_1 + \Gamma_2 \neq 0$. The first step of the procedure defines two new complex coordinates and two new vorticities used to define the Poisson bracket and equations of motion.

$$\begin{aligned} \tilde{z}_1 &= z_1 - z_2; & \tilde{\Gamma}_1 &= \frac{\Gamma_1\Gamma_2}{\Gamma_1 + \Gamma_2}; \\ \tilde{z}_2 &= \frac{\Gamma_1 z_1 + \Gamma_2 z_2}{\Gamma_1 + \Gamma_2}; & \tilde{\Gamma}_2 &= \Gamma_1 + \Gamma_2; \\ \tilde{z}_3 &= z_3; & \tilde{\Gamma}_3 &= \Gamma_3. \end{aligned} \tag{2.16}$$

Letting

$$\tilde{H}(\tilde{\mathbf{z}}) = H(\mathbf{z}(\tilde{\mathbf{z}}))\,,$$

the system evolves under a system of the form (2.11), but in the "tilde" variables and circulations. The variable $\tilde{z}_1$ is the displacement vector from z_2 to z_1, and $\tilde{z}_2$ coincides with the center of vorticity of the pair.

We perform an equivalent reduction combining $\tilde{z}_2$, $\tilde{z}_3$, and their circulations, defining Z_2 as the vector from $\tilde{z}_3$ to $\tilde{z}_2$, and Z_3 as their mutual center of vorticity, and the reduced circulations as κ_j. In terms of the

original coordinates and circulations, we find

$$
\begin{aligned}
Z_1 &= z_1 - z_2; & \kappa_1 &= \Gamma_1+\Gamma_2;\\
Z_2 &= \frac{\Gamma_1 z_1+\Gamma_2 z_2}{\Gamma_1+\Gamma_2} - z_3; & \kappa_2 &= \frac{(\Gamma_1+\Gamma_2)\Gamma_3}{\Gamma_1+\Gamma_2+\Gamma_3};\\
Z_3 &= \frac{\Gamma_1 z_1+\Gamma_2 z_2+\Gamma_3 z_3}{\Gamma_1+\Gamma_2+\Gamma_3}; & \kappa_3 &= \Gamma_1+\Gamma_2+\Gamma_3,
\end{aligned}
\tag{2.17}
$$

under the assumption that $\Gamma_1+\Gamma_2+\Gamma_3 \neq 0$, these are Jacobi coordinates. This geometric construction is shown in Fig. 2.1 for the case of three vortices with identical circulation.

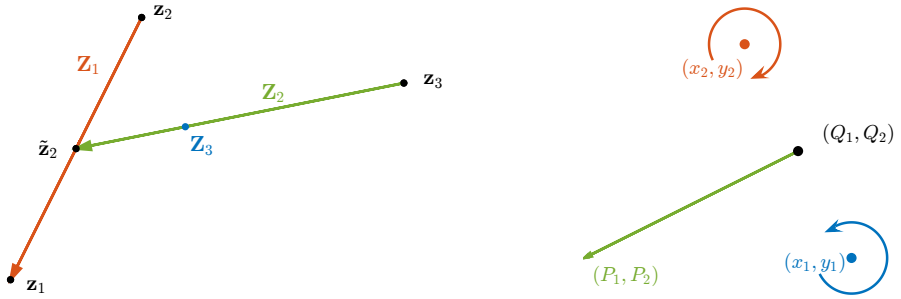

FIGURE 2.1. **Left:** Jacobi coordinates for three particles with nonzero total circulation. The coordinate $\mathbf{Z}_1$ is the vector from $\mathbf{z}_2$ to $\mathbf{z}_1$, $\mathbf{Z}_2$ is the vector from $\mathbf{z}_3$ to $\tilde{\mathbf{z}}_2$ (the center of vorticity of the first two particles), and the transformed variable $\mathbf{Z}_3$ is the conserved center of vorticity. Note carefully that the variables z_1, z_2, z_3, $\tilde{z}_2$, and Z_3 are locations in space, represented by dots, whereas Z_1 and Z_2 are displacement vectors, represented by arrows. **Right:** The alternative to Jacobi coordinates for two point-vortices with $-\Gamma_2 = \Gamma_1 > 0$.

Noting that $Z_3 = z_0$, the center of vorticity defined in Eq. (2.13), we may set it to zero without loss of generality. The definition of angular impulse Θ given by Eq. (2.12) depends on the choice of the origin of the coordinate system for the vortex positions in Eq. (2.1). Placing the origin at the center of vorticity at the origin identifies the angular impulse with the conserved quantity $L = \Theta - M_x^2 - M_y^2$ arising in Aref's approach to this problem [4] and with the Casimir for the Lie-Poisson dynamics identified by Hernández-Garduño [14].

In these coordinates, the Hamiltonian (2.3) becomes

$$
H = \frac{-\Gamma_1\Gamma_2}{2}\log|Z_1|^2 - \frac{\Gamma_2\Gamma_3}{2}\log\left|Z_2 - \frac{\kappa_1}{\Gamma_2}Z_1\right|^2 - \frac{\Gamma_1\Gamma_3}{2}\log\left|Z_2 + \frac{\kappa_1}{\Gamma_1}Z_1\right|^2,
\tag{2.18}
$$

and

$$
\Theta = \kappa_1|Z_1|^2 + \kappa_2|Z_2|^2.
\tag{2.19}
$$

The Poisson bracket and evolution equations in these variables depend on the *virtual positions* Z_1 and Z_2 and the *virtual circulations* κ_1 and κ_2 in the same way that equations (2.2) and (2.9) depend on the physical positions z_j circulations Γ_j. As such, we define the matrix

$$
\mathsf{D}_\kappa := \operatorname{diag}(\kappa_1, \kappa_2).
\tag{2.20}
$$

A principal advantage of the Jacobi reduction is that it maintains the diagonal form of the matrix D_κ. Other, more algebraically straightforward reductions can produce a reduced symplectic form (2.6) defined in terms of a dense matrix instead [27].

The change to Jacobi coordinates depends on the order of the labels assigned to the point vortices. All such reductions lead to equivalent systems, but some may be more convenient to work with than others. If

the circulations sum to zero, then the final application of Eq. (2.16) is undefined because the two fractions appearing in that equation have vanishing denominators. We discuss this case in Sec. 5.

2.2. **Reduction to Lie-Poisson form.** The above reduction mods out translations in $\mathbb{C}^3$, but the evolution in $\mathbf{Z} = (Z_1, Z_2)^\mathsf{T}$ is still invariant under $\mathbb{S}^1$ action on $\mathbb{C}^2$,

$$\mathbb{S}^1 \times \mathbb{C}^2 \to \mathbb{C}^2;\ \left(e^{\mathrm{i}\psi}, \mathbf{Z}\right) \mapsto e^{\mathrm{i}\psi}\mathbf{Z}. \tag{2.21}$$

The following change of variables is motivated by the fact that the Hamiltonian (2.18) depends on the coordinates only through the combinations $|Z_1|^2$, $|Z_2|^2$, $Z_1 Z_2^*$, and $Z_1^* Z_2$. The *momentum map* is the function

$$\mathbf{J} : \mathbb{C}^2 \to \mathfrak{u}(2); \quad \mathbf{Z} \mapsto \mu = \mathrm{i}\mathbf{Z}\mathbf{Z}^* = \mathrm{i}\begin{bmatrix} |Z_1|^2 & Z_1 Z_2^* \\ Z_1^* Z_2 & |Z_2|^2 \end{bmatrix}, \tag{2.22}$$

where the asterisk represents the Hermitian transpose of a vector or matrix. The momentum map sends complex vectors to skew-Hermitian matrices, i.e., those satisfying $\mu^* = -\mu$.

Since the Hamiltonian is invariant to $\mathbb{S}^1$ transformations of the form (2.21), it can be defined entirely in terms of elements of the matrix μ. Thus we may write the Hamiltonian as $h(\mu)$, where

$$H = h \circ \mathbf{J}.$$

Then μ can be shown to satisfy the evolution equation

$$\dot{\mu} = \mathsf{D}_\kappa^{-1} \frac{\delta h}{\delta \mu}\mu - \mu \frac{\delta h}{\delta \mu}\mathsf{D}_\kappa^{-1}. \tag{2.23}$$

This can be interpreted as a Hamiltonian system because this change of variables is a Poisson transformation, which we explain below. For the reader who simply wants to perform the change of variables, Eqs. (2.22) and (2.23) are practically the whole story once we define the functional derivative $\frac{\delta h}{\delta \mu}$, which we do in Eqs. (2.26)–(2.28) after introducing some additional machinery.

We refer to Ohsawa [26–28] for the derivation, a detailed interpretation, and an application of this reduction to several stability problems in vortex dynamics, and to Marsden and Ratiu for the necessary background in geometric mechanics [22]. Here, we try to explain where this comes from with the minimal possible detail. First, define $\mathfrak{u}(2)_\kappa$ as the vector space of skew-Hermitian 2×2 matrices equipped with the bracket

$$[\xi, \eta]_\kappa = \xi \mathsf{D}_\kappa^{-1} \eta - \eta \mathsf{D}_\kappa^{-1} \xi,$$

an antisymmetric bilinear operator that satisfies the Jacobi identity, making $\mathfrak{u}(2)_\kappa$ a Lie algebra.

Next, define the inner product

$$\langle \xi, \eta \rangle = \frac{1}{2}\operatorname{tr}(\xi^* \eta). \tag{2.24}$$

Now, $\mathfrak{u}(2)_\kappa^*$, the dual of $\mathfrak{u}(2)_\kappa$, is the set of all linear operators on $\mathfrak{u}(2)_\kappa$, and can be identified in a one-one manner with elements of $\mathfrak{u}(2)_\kappa$. That is, if $\alpha \in \mathfrak{u}(2)_\kappa^*$, there exists a unique $\alpha^\sharp \in \mathfrak{u}(2)_\kappa$ such that

$$\alpha(\mu) = \langle \alpha^\sharp, \mu \rangle$$

for all $\mu \in \mathfrak{u}(2)_\kappa$.

This allows us to define a Lie-Poisson bracket on pairs of functions in $\mathfrak{u}(2)_\kappa^* \cong \mathfrak{u}(2)_\kappa$,

$$\{f, g\}_\kappa(\mu) := \left\langle \mu, \left[\frac{\delta f}{\delta \mu}, \frac{\delta g}{\delta \mu}\right]_\kappa \right\rangle \tag{2.25}$$

using the inner product (2.24). With these definitions in hand, we return to our definition of the momentum map in Eq. (2.22) and note that the codomain is properly defined as $\mathfrak{u}(2)_\kappa^*$, because, as discussed in [22], this bracket is defined on the dual of a Lie algebra.

The functional derivatives are defined such that for any $\mu, \nu \in \mathfrak{u}(2)^*_\kappa$

$$\left\langle \nu, \frac{\delta f}{\delta \mu} \right\rangle = \left. \frac{\mathrm{d}}{\mathrm{d}s} \right|_{s=0} f(\mu + s\nu). \tag{2.26}$$

For an element $\mu \in \mathfrak{u}(2)^*_\kappa$ of the form

$$\mu = \mathrm{i} \begin{bmatrix} \mu_1 & \mu_3 + \mathrm{i}\mu_4 \\ \mu_3 - \mathrm{i}\mu_4 & \mu_2 \end{bmatrix}, \tag{2.27}$$

this gives

$$\frac{\delta f}{\delta \mu} = \mathrm{i} \begin{bmatrix} 2\frac{\partial f}{\partial \mu_1} & \frac{\partial f}{\partial \mu_3} + \mathrm{i}\frac{\partial f}{\partial \mu_4} \\ \frac{\partial f}{\partial \mu_3} - \mathrm{i}\frac{\partial f}{\partial \mu_4} & 2\frac{\partial f}{\partial \mu_2} \end{bmatrix}. \tag{2.28}$$

Putting this all together, we can now say precisely how the momentum map is canonical. It is a *Poisson map* with respect to the Poisson brackets (2.9) and (2.25), meaning that

$$\{f \circ \mathbf{J}, h \circ \mathbf{J}\} = \{f, h\}_\kappa \circ \mathbf{J}.$$

Therefore, any smooth function $f(\mu)$ evolves under

$$\frac{\mathrm{d}}{\mathrm{d}t} f(\mu) = \{f, h\}_\kappa.$$

Applying this to the components of μ gives the evolution equation (2.23).

Since μ is defined as the exterior product of two vectors, it has rank at most one. Therefore, the two rows are redundant. To take practical advantage of this fact, note that its determinant must vanish. For matrix (2.27), this results in the single real equation

$$\mu_1 \mu_2 - \mu_3^2 - \mu_4^2 = 0. \tag{2.29}$$

To interpret the μ_j coordinates geometrically, consider the triangle formed by the variables Z_1 and Z_2 interpreted as vectors in $\mathbb{R}^2$. Writing $Z_j = R_j e^{\mathrm{i}\phi_j}$ and $\phi = \phi_1 - \phi_2$, we see

$$\mu_1 = R_1^2, \qquad \mu_2 = R_2^2, \qquad \mu_3 = R_1 R_2 \cos\phi, \qquad \mu_4 = R_1 R_2 \sin\phi. \tag{2.30}$$

Thus, μ_4 is the signed area of the triangle with sides R_1 and R_2, and μ_3 is the inner product of these vectors.

In these variables, the angular impulse (2.19) is

$$\Theta = \kappa_1 \mu_1 + \kappa_2 \mu_2. \tag{2.31}$$

and we may consider the evolution equations (2.23) as describing the behavior of a vector in $\mathbb{R}^4$. Since, as we will see below in Eq. (2.35), $\frac{\partial h}{\partial \mu_4} = 0$, μ evolves according to

$$\frac{\mathrm{d}\mu}{\mathrm{d}t} = \begin{bmatrix} \frac{2}{\kappa_1}\frac{\partial h}{\partial \mu_3}\mu_4 \\ -\frac{2}{\kappa_2}\frac{\partial h}{\partial \mu_3}\mu_4 \\ 2\left(\frac{\frac{\partial h}{\partial \mu_2}}{\kappa_2} - \frac{\frac{\partial h}{\partial \mu_1}}{\kappa_1}\right)\mu_4 \\ 2\mu_3\left(\frac{\frac{\partial h}{\partial \mu_1}}{\kappa_1} - \frac{\frac{\partial h}{\partial \mu_2}}{\kappa_2}\right) + \frac{\partial h}{\partial \mu_3}\left(\frac{\mu_2}{\kappa_1} - \frac{\mu_1}{\kappa_2}\right) \end{bmatrix}. \tag{2.32}$$

Since Θ is conserved, as is apparent from the first two components of system (2.32), it is worthwhile to make one more change of variables, defining

$$Z := \kappa_1 \mu_1 - \kappa_2 \mu_2 \quad \text{and} \quad X + \mathrm{i}Y := \mu_3 + \mathrm{i}\mu_4. \tag{2.33}$$

Then, the rank-one condition (2.29) becomes

$$\Theta^2 = Z^2 + 4\kappa_1\kappa_2\left(X^2 + Y^2\right) = Z^2 + \frac{4\gamma_3}{\gamma_1}\left(X^2 + Y^2\right), \tag{2.34}$$

where the symmetric variables γ_1 and γ_3 are defined in Eq. (2.14). Since Θ is conserved, trajectories are constrained to a quadric surface in three-dimensional (X,Y,Z) space. Without loss of generality, we may assume $\gamma_1 > 0$. The surface is a spheroid if one or three circulations are positive and one sheet of a two-sheeted hyperboloid of rotation if two are positive.[1] In the spheroidal case, $\Theta > 0$, and Z may take either sign. In the hyperboloidal case, $\gamma_3 < 0$, which implies $Z > 0$, but permits Θ to take either sign. In the case $\Theta = 0$, the hyperboloidal surface degenerates to an upper half-cone. The distinction between spheroidal and hyperboloidal phase surfaces was noted in Ref. [14, 15] using action-angle coordinates for Z_1 and Z_2.

Using the notation (2.14), we may write the Hamiltonian as

$$\begin{aligned} h(X,Y,Z;\Theta) = &-\frac{\Gamma_1\Gamma_2}{2}\log\left(Z+\Theta\right) \\ &-\frac{\Gamma_1\Gamma_3}{2}\log\left(\quad 4\gamma_3 X+(\gamma_1\Gamma_1-\Gamma_2\Gamma_3)Z+(\Gamma_1+\Gamma_2)\left(\Gamma_1+\Gamma_3\right)\Theta\right) \\ &-\frac{\Gamma_2\Gamma_3}{2}\log\left(-4\gamma_3 X+(\gamma_1\Gamma_2-\Gamma_1\Gamma_3)Z+(\Gamma_1+\Gamma_2)\left(\Gamma_2+\Gamma_3\right)\Theta\right), \end{aligned} \tag{2.35}$$

yielding evolution equations, again, using $\frac{\partial h}{\partial Y} = 0$,

$$\frac{\mathrm{d}}{\mathrm{d}t}\begin{bmatrix} X \\ Y \\ Z \end{bmatrix} := \mathbf{F}(X,Y,Z) = \begin{bmatrix} -4h_Z Y \\ 4h_Z X - \frac{\gamma_1}{\gamma_3}h_X Z \\ 4h_X Y \end{bmatrix}. \tag{2.36}$$

This formula is valid regardless of sign γ_3 and thus unifies the two systems of equations derived in [1]. This system, like those, can be shown to be a *Nambu bracket* formulation of the equations, defined in terms of the Casimir Θ.

We note the Hamiltonian (2.35) is singular when two vortices collide and the argument of the corresponding logarithmic term vanishes. The three singularities all occur for $Y = 0$ and must also solve (2.34). We list them for later reference:

$$\begin{aligned} \mathscr{S}_{12} &= (0,0,-\Theta), \\ \mathscr{S}_{13} &= \left(\frac{-\gamma_1\Theta}{(\Gamma_1+\Gamma_2)(\Gamma_1+\Gamma_3)}, 0, \frac{(\gamma_1\Gamma_1-\Gamma_2\Gamma_3)\Theta}{(\Gamma_1+\Gamma_2)(\Gamma_1+\Gamma_3)}\right), \\ \mathscr{S}_{23} &= \left(\frac{\gamma_1\Theta}{(\Gamma_1+\Gamma_2)(\Gamma_2+\Gamma_3)}, 0, \frac{(\gamma_1\Gamma_2-\Gamma_1\Gamma_3)\Theta}{(\Gamma_1+\Gamma_2)(\Gamma_2+\Gamma_3)}\right). \end{aligned} \tag{2.37}$$

The subscripts indicate which two vortices' positions coincide at the singularities. The location of the singularities diverges if any pair of circulations satisfies $\Gamma_j + \Gamma_k \to 0$.

3. Local and global bifurcations

Relative fixed points of system (2.2) are fixed points of system (2.36). It is well-known that the three-vortex system has two families of relative fixed points: equilateral triangular configurations and collinear configurations. We consider these in turn.

Central to this work, we rely on a kind of bifurcation diagram introduced by Conte in his 1979 Thèse d'État and expounded upon by the same author in a later publication and by Aref [4, 10, 11]; see Fig. 3.1. The analysis below allows us to explain this diagram more simply than previous authors and to extend its reach. We assume $\gamma_1 \neq 0$ and define scaled circulations

$$\eta_j = \frac{\Gamma_j}{\gamma_1}, j = 1,\ldots,3, \tag{3.1}$$

[1] Recall that a spheroid is an ellipsoid with two equal axes, and a hyperboloid of rotation is a hyperboloid with two equal axes.

so that

$$\eta_1 + \eta_2 + \eta_3 = 1. \tag{3.2}$$

As such, the scaled circulations η_j may be interpreted as *affine coordinates* for the parameter plane. That is, given three points (x_j, y_j) in the plane, then any point in $\mathbb{R}^2$ can be written as

$$(x,y) = \sum_{j=1}^{3} \eta_j \cdot (x_j, y_j).$$

Placing the three points at the vertices of an equilateral triangle is a common choice whose symmetries help highlight the invariance of the system to permutations of the vortices' labels. More details of the coordinates are given in Appendix B.

In these variables, the condition that the phase surface is a spheroid is $\eta_1\eta_2\eta_3 > 0$, corresponding to the figure's shaded regions. By contrast, the phase surface is a hyperboloid in the unshaded areas.

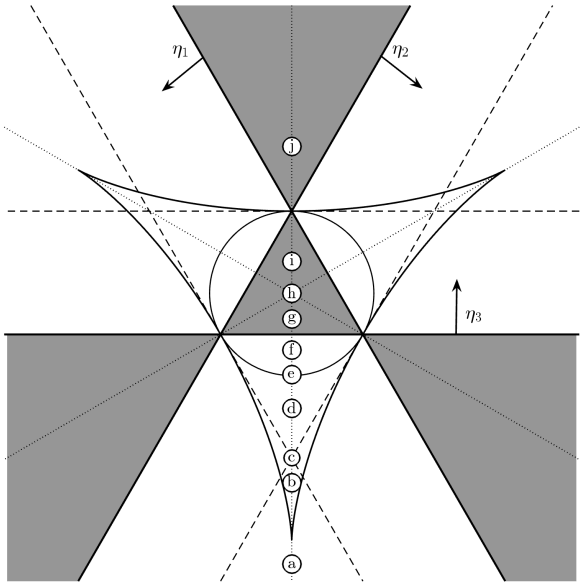

FIGURE 3.1. The trilinear diagram identifying regimes of phase space behavior. The three arrows point to the direction in which the indicated scaled circulation is positive so that each vanishes on the line the arrow emerges from. In the shaded region, the quadric surface defining the phase space (hereafter, the *phase surface*) in Eq. (2.34) is a spheroid, and in the unshaded region, it is a hyperboloid.

To determine the linear stability of an equilibrium, we must linearize the system (2.36) about it. The Jacobian of this matrix is

$$D\mathbf{F} = \begin{bmatrix} -4h_{XZ}Y & -4h_Z & -4h_{ZZ}Y \\ \frac{-\gamma_1}{\gamma_3}h_{XX}Z + 4\left(h_{XZ}X + h_Z\right) & 0 & \frac{-\gamma_1}{\gamma_3}\left(h_X + h_{XZ}Z\right) + 4h_{ZZ}X \\ 4h_{XX}Y & 4h_X & 4h_{XZ}Y \end{bmatrix}, \tag{3.3}$$

where subscripts denote partial derivatives. Its trace is identically zero and its determinant is

(3.4)
$$\det D\mathbf{F} = -16Y\left(\frac{\gamma_1 h_X}{\gamma_3}\left(h_X h_{XZ} - h_{XX}(h_Z + h_{ZZ}Z) + h_{XZ}^2 Z\right) + 4h_Z\left(h_{ZZ}(h_X + h_{XX}X) - h_{XZ}^2 X - h_{XZ}h_Z\right)\right).$$

3.1. **Equilateral configurations.** When $Y = 0$, the three equations are collinear, so the equilateral configurations must have $Y \neq 0$. These solutions must satisfy $h_X = h_Z = 0$ and the rank-one condition (2.34). Solving these three equations yields two solutions

$$\mathscr{E}_{\text{tri}}^{\pm} = \frac{\Theta}{\gamma_2}\left(\frac{(\Gamma_1 - \Gamma_2)\gamma_1}{2(\Gamma_1 + \Gamma_2)}, \pm\frac{\sqrt{3}\gamma_1}{2}, \Gamma_1\Gamma_2 - \frac{\left(\Gamma_1^2 + \Gamma_2^2\right)\Gamma_3}{\Gamma_1 + \Gamma_2}\right). \tag{3.5}$$

These fixed points diverge as $\gamma_2 \to 0$. The equation $\gamma_2 = 0$ corresponds to the circle circumscribing the central shaded triangle in Fig. 3.1.

Linearizing about this solution, we find the Jacobian (3.3) has characteristic polynomial

$$\chi_{\text{tri}}(\lambda) = -\lambda^3 - \frac{3\gamma_2^3}{\Theta^2\gamma_1^2}\lambda. \tag{3.6}$$

The quadratic term vanishes because $\operatorname{tr} D\mathbf{F} \equiv 0$ and the constant term vanishes because the determinant (3.4) vanishes when $h_X = h_Z = 0$. This always has one eigenvalue $\lambda = 0$. The other two eigenvalues indicate linear stability if $\gamma_2 > 0$ (inside the circle) and instability if $\gamma_2 < 0$ (outside the circle).

3.1.1. *Collinear configurations.* On all collinear configurations, $Y = 0$, so that $\frac{\mathrm{d}X}{\mathrm{d}t}$ and $\frac{\mathrm{d}Z}{\mathrm{d}t}$ identically vanish by Eq. (2.36). Thus, such configurations must satisfy both $\frac{\mathrm{d}Y}{\mathrm{d}t} = 0$ and the rank-one condition (2.34) with $Y = 0$. These are both rational equations in X and Z; thus, their roots satisfy polynomial equations.

We may eliminate X from this system by computing the *resultant* of these two polynomials using Mathematica, as described in Sec. A, yielding the condition

$$\rho(Z;\Gamma_1,\Gamma_2,\Gamma_3,\Theta) = -64\gamma_1\gamma_3^2(Z - Z_{12})(Z - Z_{13})(Z - Z_{23})\, p_3(Z;\Theta,\Gamma_1,\Gamma_2,\Gamma_3), \tag{3.7}$$

where the Z_{ij} terms are the Z-components of singularities found in Eq. (2.37) and p_3 is a cubic polynomial in Z with Θ and the three circulations appearing as parameters. The three singularities cannot be solutions, so the system will have one or three real roots, except at bifurcation points where there are two.

The number of solutions changes at parameter values where the *discriminant* of $p_3(Z)$, which is proportional to the resultant of p_3 and p_3', vanishes; this is also reviewed in Appendix A. We compute this in Mathematica. It factors into the product of low-degree terms that we can interpret:

$$\operatorname{Disc}_{p_3}(\Gamma_1,\Gamma_2,\Gamma_3) = 64\Theta^6(\Gamma_1 - \Gamma_2)^2(\Gamma_1 + \Gamma_2)^2\,{\gamma_1}^2{\gamma_2}^2{\gamma_3}^6\left(32\gamma_2{\gamma_1}^2 - 36\gamma_3\gamma_1 - 3{\gamma_2}^2\right). \tag{3.8}$$

We review each factor below.

The factor Θ^6. When $\Theta \neq 0$, the evolution equations (2.36) depend on X, Y, and Z only through terms of the form $\frac{X}{\Theta}$, $\frac{Y}{\Theta}$, and $\frac{Z}{\Theta}$, so, for fixed values of the circulations, the phase space and fixed points scale with Θ as long as $\operatorname{sign}(\Theta)$ remains unchanged. This reflects the scale invariance of the general N-vortex problem. As remarked above, when the conservation law (2.34) represents a spheroid, then $\Theta > 0$, but when it represents a hyperboloid, Θ may take either sign or equal zero, and there are three families of phase planes.

The factors $(\Gamma_1 - \Gamma_2)^2(\Gamma_1 + \Gamma_2)^2$. Since the system of equations is invariant under permutations of the circulations, the bifurcations's locations must depend on the circulations only through the symmetric polynomials, so any factors that depend on non-symmetric combinations of the circulations must be an artifact of the reduction method and do not indicate bifurcations. Recall that the vanishing discriminant is necessary but insufficient for the two polynomials to vanish jointly. In particular, the null vector may not be of the form given in Eq. (A.1).

The factor ${\gamma_2}^2$. This vanishes at the same points where we found the equilateral configurations change stability: the circle in Fig. 3.1. Since this term is a perfect square, the discriminant vanishes on the circle but does not change signs, and the number of solutions does not change, except at the three points where the circle and deltoid (defined below) are tangent. However, as the circle is approached at other points, two collinear relative equilibria diverge to infinity.

The factor ${\gamma_3}^6$. We may expand this factor as ${\Gamma_1}^6{\Gamma_2}^6{\Gamma_3}^6$. Thus, it vanishes when any circulations vanish, but it does not change signs as the circulations cross these lines since each is raised to an even power. Crossing these lines, the phase-surface topology changes from a spheroid to a hyperboloid.

The factor $\left(32{\gamma_1}^2\gamma_2 - 36\gamma_3\gamma_1 - 3{\gamma_2}^2\right)$. This factor is quartic in the circulations. In Fig. 3.1, the locus of solutions looks like a curved triangle with cusps at the three corners. It is a well-known curve called the deltoid or Steiner's hypocycloid, defined as the image of a point on the circumference of a circle of radius one that rolls without slipping along the inside of a circle of radius three. We confirmed this by calculating the explicit form of the curve as a function of the Cartesian (x,y) variables needed to pass this curve to the plotting software. Inside the deltoid, the system has three collinear equilibria; outside, it has only one. If the triple of circulations crosses the deltoid at any point other than the cusps or the vertices of the central triangular region, two equilibria undergo saddle node-bifurcation. The bifurcation is a pitchfork if the triple crosses through the cusp along the deltoid's symmetry axis. This is the generic behavior of the *cusp catastrophe*.

Along the three lines where two circulations are equal and opposite, the number of fixed points decreases by one. As these lines are approached, one equilibrium diverges to infinity.

Linear Stability. Plugging $Y = 0$ into the Jacobian (3.3), the four entries at the corners of the matrix vanish identically, leaving a characteristic polynomial of the form

$$\chi_{\text{coll}}(\lambda) = -\lambda^3 - r(\mathscr{E})\lambda, \tag{3.9}$$

where

$$r(\mathscr{E}) = \frac{-4\gamma_1}{\gamma_3}\left((h_X)^2 + h_X h_{XZ} Z - h_{XX} h_Z Z\right) - 16\left(-h_X h_{ZZ} X + h_{XZ} h_Z X + (h_Z)^2\right)$$

is a rational function in X and Z whose coefficients depend on Θ and the circulations Γ_j. An equilibrium $\mathscr{E}$ is stable when $r(\mathscr{E}) > 0$.

The collinear fixed points correspond to the roots of the cubic polynomial $p_3(Z)$ defined in Eq. (3.7). While this is formally solvable via Cardano's formula, the resulting expressions are too complicated to be practically useful. Therefore, we cannot hope to evaluate $r(\mathscr{E})$ at a collinear equilibrium to obtain a simple stability criterion as we did in Eq. (3.6) for the triangular equilibria.

Instead, we can search for values of the circulations where the stability changes. At such equilibria, $Y = 0$, and the remaining components X and Z must satisfy three equations: the rank-one condition (2.34), $\frac{\mathrm{d}Y}{\mathrm{d}t} = 0$, and $r(\mathscr{E}) = 0$. We may eliminate X and Z from this system by computing three resultants. First, choose two pairs of equations and eliminate X from each pair with a resultant, producing two equations in Z alone. Then, compute a third resultant to eliminate Z from the first two resultants. Doing so in Mathematica, we find this final resultant condition takes the form

$$\Theta^{24} p_{30}(\Gamma_1,\Gamma_2,\Gamma_3)(\Gamma_1+\Gamma_2)^2(\Gamma_1+\Gamma_3)^2(\Gamma_2+\Gamma_3)^2\,{\gamma_1}^{16}{\gamma_2}^4{\gamma_3}^{24}\left(32\gamma_2{\gamma_1}^2 - 36\gamma_3\gamma_1 - 3{\gamma_2}^2\right) = 0. \tag{3.10}$$

All the factors are symmetric in the three circulations except for $p_{30}(\Gamma_1,\Gamma_2,\Gamma_3)$, a degree-30 homogeneous polynomial in the circulations. Like the $(\Gamma_1-\Gamma_2)^2(\Gamma_1+\Gamma_2)^2$ terms found in the discriminant formula above, zeros of p_{30} do not correspond to meaningful bifurcations, since p_{30} does not depend symmetrically on the circulations.

The factors ${\gamma_1}^{16}{\gamma_2}^4{\gamma_3}^{24}\left(32\gamma_2{\gamma_1}^2 - 36\gamma_3\gamma_1 - 3{\gamma_2}^2\right)$ vanish on the same sets as the discriminant (3.8). The only new symmetric factor that arises in Eq. (3.10) but is not present in the discriminant is

$$(\Gamma_1+\Gamma_2)^2(\Gamma_1+\Gamma_3)^2(\Gamma_2+\Gamma_3)^2.$$

This vanishes when two vortices have equal and opposite circulation and can form a dipole. This occurs on the three dashed lines in Fig. 3.1. As these lines are approached, two collinear fixed points diverge to infinity. However, this factor does not change signs on these lines and thus does not lead to a change in stability.

3.1.2. *The collinear equilibria when* $\Gamma_1 = \Gamma_2$. We can obtain more explicit results, which help our intuition by making the additional assumption $\Gamma_1 = \Gamma_2$. This occurs along the y-axis in the diagram of Fig. 3.1. For simplicity, we also assume $\gamma_1 = 1$ so that $\Gamma_1 = \Gamma_2 = \frac{1-\Gamma_3}{2}$. The cubic polynomial $p_3(Z)$ that appears in the resultant (3.7) factors into a linear term and a quadratic term, enabling us to find the three equilibria

$$
\begin{aligned}
\mathscr{E}_1 &= \frac{\Theta}{(1+\Gamma_3)(1+3\Gamma_3)}\left(\sqrt{\frac{5+3\Gamma_3}{1-\Gamma_3}}, 0, -3\Gamma_3^2 - 6\Gamma_3 + 1 \right) \\
\mathscr{E}_2 &= \frac{\Theta}{(1+\Gamma_3)(1+3\Gamma_3)}\left(-\sqrt{\frac{5+3\Gamma_3}{1-\Gamma_3}}, 0, -3\Gamma_3^2 - 6\Gamma_3 + 1 \right) \\
\mathscr{E}_3 &= (0, 0, \Theta)\,.
\end{aligned}
\tag{3.11}
$$

The equilibria $\mathscr{E}_1$ and $\mathscr{E}_2$ only exist when the term inside the square root is positive, that is, when $\frac{-5}{3} < \Gamma_3 < 1$. Recall from the paragraph following Eq. (2.34) that in the hyperboloid case Z must be non-negative, so that $\mathscr{E}_3$ exists for $\Theta \geq 0$. The value $\Gamma_3 = \frac{-5}{3}$ occurs at the deltoid's cusp on the y-axis in Fig. 3.1 and $\Gamma_3 = 1$ occurs at the upper edge of the deltoid where it intersects the y-axis. At this upper point the circulations Γ_1 and Γ_2 vanish, so the system degenerates to one-vortex problem.

We remark on the Θ-dependence of these solutions. From the discussion following Eq. (2.34), in the case of spheroidal phase surface, i.e., for $\Gamma_3 > 0$, $\Theta > 0$, while for the case of hyperboloid phase surface, $Z > 0$, so $\mathscr{E}_3$ exists only for $\Theta > 0$, while $\mathscr{E}_1$ and $\mathscr{E}_2$ exist for $\Theta > 0$ when $\frac{-5}{3} < \Gamma_3 < -1$ and for $\Theta < 0$ when $-1 < \Gamma_3 < \frac{-1}{3}$.

The function $r(\mathscr{E})$ that determines stability in Eq. (3.9) takes the values

$$
r(\mathscr{E}_1) = r(\mathscr{E}_2) = \frac{(\Gamma_3 - 1)^2 (3\Gamma_3 + 1)^3 (3\Gamma_3 + 5)}{64\Theta^2} \quad \text{and} \quad r(\mathscr{E}_3) = \frac{3(\Gamma_3 - 1)^3 (3\Gamma_3 + 5)}{16\Theta^2}.
$$

The function $r(\mathscr{E}_1)$ is negative for $\frac{-5}{3} < \Gamma_3 < \frac{-1}{3}$, where $\mathscr{E}_1$ and $\mathscr{E}_2$ are centers, and positive for $\frac{-1}{3} < \Gamma_3 < 1$, where they are saddles. The sign of $r(\mathscr{E}_3)$ shows that $\mathscr{E}_3$ is a saddle for $\frac{-5}{3} < \Gamma_3 < 1$, inside the deltoid, and a center outside it.

Fig. 3.2 displays a bifurcation diagram for $\eta_1 = \eta_2$ and variable η_3 with separate plots for the $\Theta = -1$ and $\Theta = 1$ cases. The collinear and equilateral states are depicted, along with the singularities. The bifurcation at $\eta_3 = -1$ is a pitchfork, but all other bifurcations occur when fixed points diverge to and return from infinity, sometimes moving between the $\Theta = \pm 1$ surfaces. When $\eta_3 > 0$, the phase surface is spheroidal, so $\Theta < 0$ is not allowed.

4. Global phase portraits

In addition to the topology of the phase surface, the existence of fixed points, and their stability, the global dynamics depends on the topology of the trajectories and especially on the connecting orbit. When the solution is confined to a spheroid, all trajectories are bounded, while in the hyperboloid cases, some trajectories are unbounded in certain cases. The phase-space topology also depends on the connections between saddles. In this section, we display representative phase planes in all regions of the diagram and on the boundaries between the regions. We start by displaying the cases along the symmetry line $\Gamma_1 = \Gamma_2$.

By a straightforward rescaling of the circulations, we may assume $\gamma_1 = 1$, in which case the distinction between the absolute circulations Γ_i and scaled circulations defined by Eq. (3.1) disappears. To keep the notation consistent with the equations for the equilibria and singularities, we use Γ_i in what follows.

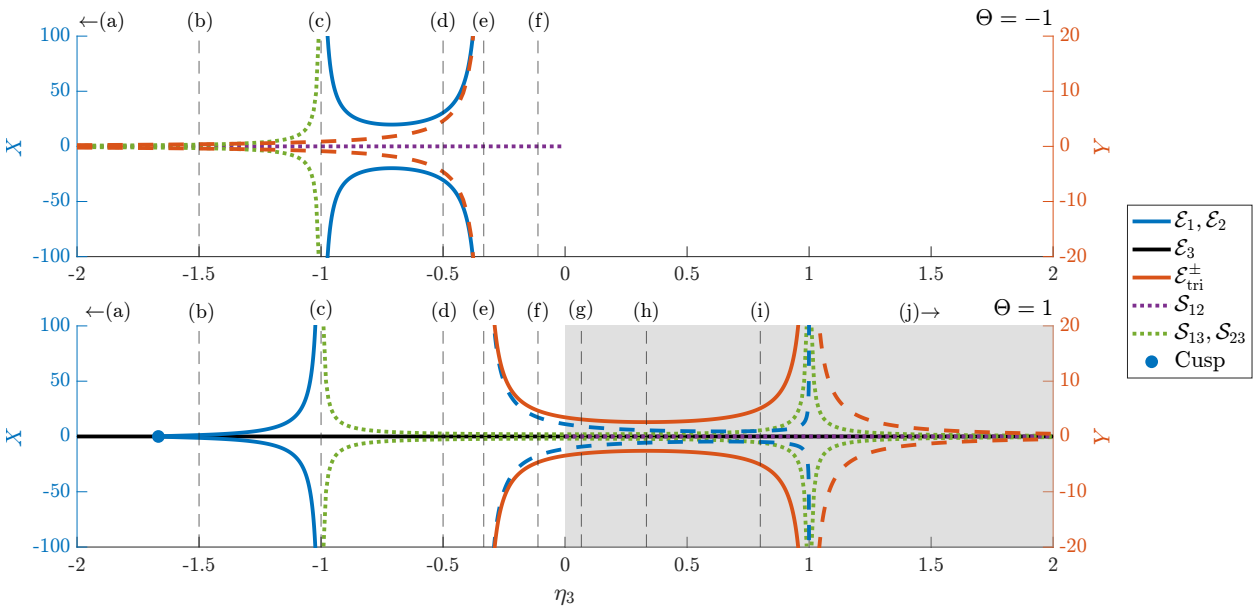

FIGURE 3.2. Bifurcation diagram displaying the equilibria and singularities defined by Eqs. (2.37), (3.5) and (3.11) for $\Theta = -1$ and $\Theta = 1$ as a function of η_3 along the vertical center line of Fig. 3.1. The X-component of the collinear equilibria and singularities is shown using the y-axis scale on the left. The Y component of the triangular equilibria is shown using the y-axis scale on the right and the same shade of red as the Y-scale along the right edge of the figure. Solid lines show stable equilibria, dashed lines show unstable equilibria, and dotted lines show singularities. Dashed vertical lines show the η_3 values indicated by the letter labels in Fig. 3.1. Cases **a** and **j** lie outside the plotted region.

In this section, we assume $\Gamma_1 = \Gamma_2 = \frac{1-\Gamma_3}{2}$, corresponding to points on the vertical symmetry axis in Fig. 3.1. We consider a sequence of points labeled **a–j** to demonstrate how the global phase space topology changes with changing Γ_3. The fixed points and singularities for this case are derived in Sec. 3.1 and 3.1.2. Along this symmetry line, the phase space is a spheroid for $\Gamma_3 > 0$ and becomes a hyperboloid for $\Gamma_3 < 0$. The phase surface is bounded in the former case, so all orbits are also necessarily bounded. In the latter, the phase surface is unbounded, but all orbits are bounded for almost all values of the circulations and the angular impulse Θ. We note the few cases where unbounded orbits exist.

We plot a sequence of phase space diagrams for varying values of Γ_3 along the symmetry line, depicting the equilibria and singularities derived in Sec. 3.1.2, the separatrix orbits emerging from any hyperbolic equilibria, and a family of periodic orbits organized by these separatrices.

The variables X and Y defined by Eq. (2.33) have simple geometric interpretations that will help us understand these phase space diagrams. First, consider Eq. (2.17). Referring to Figure 2.1, the complex variable Z_1 corresponds to the vector pointing from vortex two to vortex one, and Z_2 to the vector from vortex three to the center of circulation of the first two vortices along the symmetry line $\Gamma_1 = \Gamma_2$, it lies halfway between these two vortices. The variable Y equals the signed area of the parallelogram formed by these two vectors and thus vanishes when the three vortices are collinear. The variable X is the dot product of these two vectors and thus vanishes when they are orthogonal, which occurs when the triangle is isosceles with vortex three adjacent to the two equal sides. Note that when $\Gamma_1 \neq \Gamma_2$, this orthogonality does not imply the triangle is isosceles.

4.1. **Shperoidal Phase Surfaces.** First, we will discuss the cases for values of Γ_3 for which the dynamics lies on a spheroid, for which we may assume $\Theta = 1$. We will plot the spheroidal phase surfaces as spheres, ignoring that their axes are different lengths. We plot $Y = 0$ as the equator and the north and south poles at $Y = \pm 1$.

Point h: $\Gamma_3 = \frac{1}{3}$**.** Setting $\Gamma_3 = \frac{1}{3}$ yields the most symmetric case where all three vortices have identical circulation, the case represented by the point **h** in Fig. 3.1. Its global phase space is shown in Fig. 4.1. The system has five equilibria. The three on the equator, $\mathscr{E}_1$, $\mathscr{E}_2$, and $\mathscr{E}_3$ represent collinear states. Because the three vortices are equal, they are equispaced along the equator. They are saddle points pairwise connected by heteroclinic orbits. The two equilateral fixed points $\mathscr{E}_{\text{tri}}^{\pm}$ sit at the north and south poles. The three singularities derived in Eqs. (2.37) sit on the equator midway between each pair of collinear equilibria. On the front face, the equilibrium $\mathscr{E}_3$ and the singularities $\mathscr{S}_{13}$ and $\mathscr{S}_{23}$ are visible, while on the back face the equilibria $\mathscr{E}_1$ and $\mathscr{E}_2$ and the singularity $\mathscr{S}_{12}$ are visible.

The six heteroclinic orbits divide the sphere into five families of periodic orbits. Each heterocline connects two equilibria, corresponding to an orbit that exchanges a vortex from the end of the line segment with the one at its center. A family of periodic orbits surrounds each of the singularities on the equator. This family limits to a heteroclinic cycle connecting to collinear relative equilibria. An additional family of periodic orbits surrounds each of the equilateral equilibria. These families limit to a heteroclinic cycle that visits all three collinear equilibria.

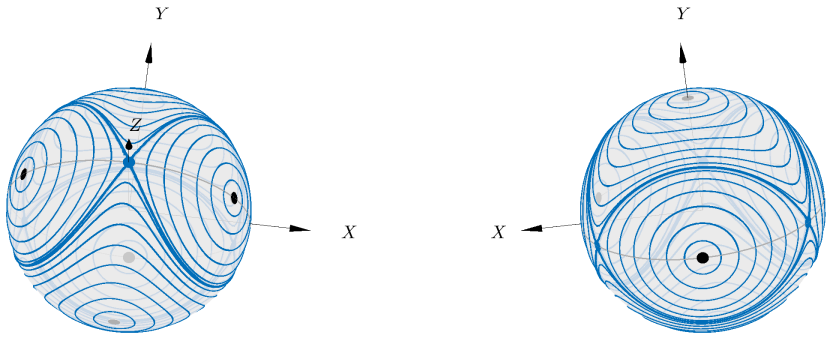

FIGURE 4.1. The global phase space for the case **h** with $\Gamma_3 = \frac{1}{3}$, showing "front" and "back" views of the sphere. The singularities are represented by black dots, the collinear equibria by blue, and the triangular equilibria by gray. The separatrix orbits are denoted by thicker curves than the periodic orbits. The equilibrium $\mathscr{E}_3$ lies on the positive Z-axis here and in all subsequent plots. The figures depict periodic orbits that are roughly equally spaced, rather than equally spacing the level sets of the Hamiltonian, which would lead to an accumulation of curves near each singularity. The markings are consistent across the remaining plots.

Point g: $\Gamma_3 = \frac{1}{15}$**.** We next move down to the point **g** in the figure, choosing $\Gamma_3 = \frac{1}{15}$; see Fig. 4.2. No local bifurcations have occurred between these two examples; the two phase-spheres differ in the topology of the periodic orbits and their limiting connecting orbits. The collinear equilibrium $\mathscr{E}_3$ now lies on a different level set of the Hamiltonian from the other two. Its invariant manifolds define a pair of homoclinic orbits, each enclosing a family of periodic orbits that limits to a singularity. Four heteroclinic orbits connect the two equilibria $\mathscr{E}_1$ and $\mathscr{E}_2$. The triangular equilibria $\mathscr{E}_{\text{tri}}^{\pm}$ have migrated toward $\mathscr{E}_3$.

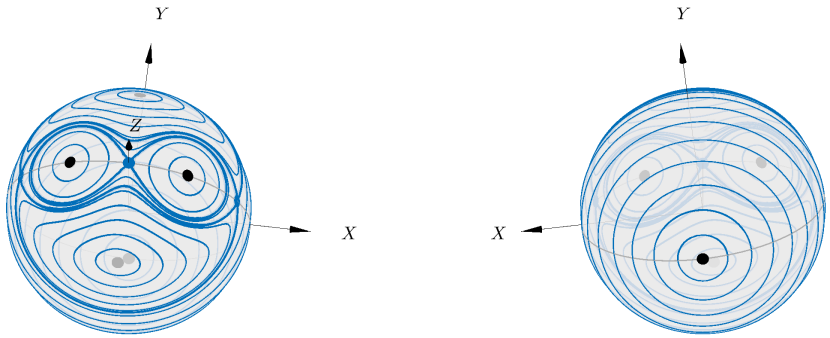

FIGURE 4.2. The global phase space for case **g** with $\Gamma_3 = \frac{1}{15}$. The invariant manifolds connected to $\mathscr{E}_3$ are homoclinic orbits oriented along the equator. The collinear equilibria $\mathscr{E}_1$ and $\mathscr{E}_2$ have migrated to the front.

Point i: $\Gamma_3 = \frac{4}{5}$**.** Moving to the point **i** in the figure, see Fig. 4.3 we see that, like at point **g**, a pair of homoclinic orbits issues from $\mathscr{E}_1$. In this case, however, they are oriented longitudinally, and each encloses a triangular equlibrium $\mathscr{E}^{\pm}_{\text{tri}}$. Four heteroclinic orbits again connect the equilibria $\mathscr{E}_1$ and $\mathscr{E}_2$, but their configuration has changed compared to point **g**. The equilibria $\mathscr{E}^{\pm}_{\text{tri}}$, $\mathscr{E}_1$ and $\mathscr{E}_2$ have all moved to the back side of the phase space sphere. As Γ_3 continues towards 1, these all converge toward the equilibrium $\mathscr{E}_3$ when the phase surface is normalized to be a unit sphere; they diverge, however, in the absolute coordinates, as seen from Eqs. (3.5) and (3.11).

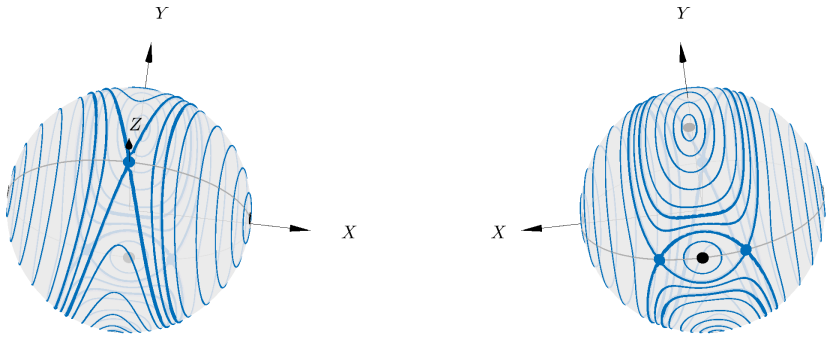

FIGURE 4.3. The global phase space for case **i** with $\Gamma_3 = \frac{4}{5}$, showing a reorganization of the homoclinic and heteroclinic structure compared to previous images.

Point j: $\Gamma_3 > 1$**.** The global phase space for $\Gamma_3 = 5$ is shown in Fig. 4.4. At $\Gamma_3 = 1$, $\Gamma_1 = \Gamma_2 = 0$, so the motion degenerates to that of a single vortex. As Γ_3 crosses 1, the parameters move from the central shaded triangle in Fig. 3.1 to the unbounded shaded region above it. The collinear equilibria $\mathscr{E}_1$ and $\mathscr{E}_2$ disappear, since they only exist inside the deltoid region. The triangular equilibria $\mathscr{E}^{\pm}_{\text{tri}}$ change from centers to saddles, as this bifurcation occurs on the circle. Heteroclinic cycles connecting $\mathscr{E}^{\pm}_{\text{tri}}$ encircle each of the three collinear singularities and the families of periodic orbits surrounding them. The stability of the remaining collinear equilibrium has also changed from unstable to stable, surrounded by periodic orbits.

4.2. **Hyperboloid phase surfaces.** As Γ_3 crosses zero, the circulation parameters move into the unshaded region of the diagram in Fig. 3.1 corresponding to a hyperboloid phase surface. We project this surface to

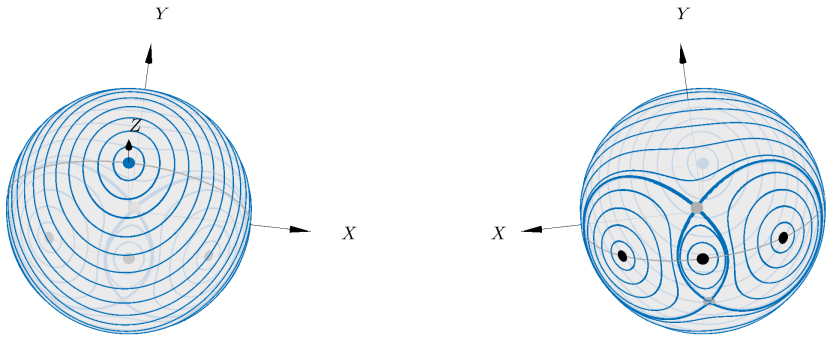

FIGURE 4.4. The global phase space for the case **j** with $\Gamma_3 = 5$. Only the single collinear equilibrium $\mathscr{E}_3$ remains and is a center. The two equilateral triangular equilibria $\mathscr{E}_{\text{tri}}^{\pm}$ are now saddles.

$Z = 0$ and plot the resulting trajectories as a phase plane. All phase planes with $\Theta < 0$ are equivalent up to scaling. Those with $\Theta > 0$ form a second equivalence class of phase planes, while the phase plane for $\Theta = 0$ is distinct. Thus, for each value of Γ_3, we plot three phase planes, one for each case. The three vortices are arranged collinearly on the line $Y = 0$ and form an isosceles triangle with vortex three at its apex on the line $X = 0$. As discussed following Eq. (3.11), the sign of Θ determines the existence of the various equilibria and singularities.

Point f: $\Gamma_3 = \frac{-1}{9}$. The phase plane for the case **f** with $\Gamma_3 = \frac{-1}{9}$ is shown in Fig. 4.5. he dynamics for $\Theta < 0$ resembles the back face of the sphere, with periodic orbits surrounding the singularity $\mathscr{S}_{12}$. The dynamics for $\Theta > 0$ closely resembles that on the "front face" of the phase sphere in the case **g** pictured in Fig. 4.2. It features the two equilateral equilibria, which are stable, and the three unstable collinear equilibria, as well as the singularities $\mathscr{S}_{13}$ and $\mathscr{S}_{23}$. T

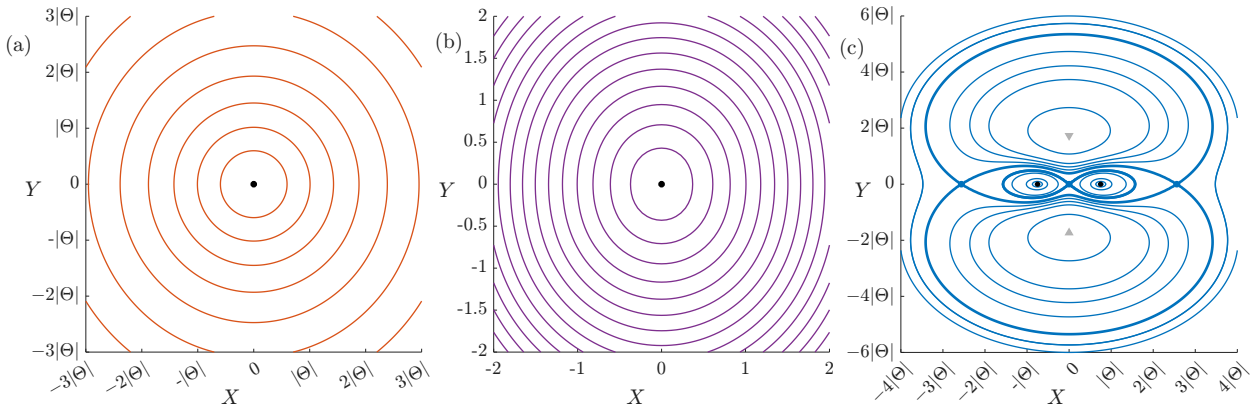

FIGURE 4.5. The XY phase planes in case **f** with $\Gamma_3 = \frac{-1}{9}$. (a) The case $\Theta < 0$. (b) The case $\Theta = 0$. (c) The case $\Theta > 0$. Markings are similar to the spherical case: Gray triangles mark the equilateral equilibria; black dots mark the singularities, and blue (or red) dots mark collinear equilibria.

Point e: $\Gamma_3 = \frac{-1}{3}$. Point **e** lies on the circle $\gamma_2 = 0$ in Fig. 3.1. This case is important because, at this parameter value, solutions that collapse in finite time are observed. As this point is approached, the radius of the triangular equilibria diverges by Eq. (3.5), and their stability type changes by Eq. (3.6). Similarly, the

two collinear equilibria $\mathscr{E}_1$ and $\mathscr{E}_2$ diverge, and their stability also changes. Therefore, exactly on this circle, the number of fixed points decreases from five to one, with only the saddle point $\mathscr{E}_3$ remaining. This is seen by comparing the plot for $\Theta > 0$ in Fig. 4.6

Earlier literature has noted that $\gamma_2 = 0$ is a necessary condition for finite-time collapse [2, 13, 19]. This occurs when $\Theta = 0$. At this value, the system has unbounded trajectories. The Hamiltonian takes the especially simple form

$$H = \frac{1}{9}\log\left(\frac{4Z^2 - 3X^2}{Z^2}\right). \tag{4.1}$$

Using Eq. (2.34) with $\Theta = 0$ yields

$$H = \frac{1}{9}\log\left(\frac{X^2+4Y^2}{X^2+Y^2}\right) = \frac{1}{9}\log\left(5 - 3\cos 2\theta\right),$$

where we have made the standard polar coordinate substitution. Since this is r-independent, the level sets of H are rays through the origin. A short calculation shows that r evolves according to

$$\frac{\mathrm{d}r}{\mathrm{d}t} = \frac{2\sqrt{3}\sin 2\theta}{3\cos 2\theta - 5}.$$

Thus for (X,Y) in the first or third quadrant, $\frac{\mathrm{d}r}{\mathrm{d}t}$ is negative and constant. The solution shrinks to zero in finite time while maintaining a constant triangular profile. Similarly, in the second and fourth quadrant, the solution collapses into the origin in negative time. This is the simplest mathematical description of the phenomenon we have seen. The picture is essentially unchanged when $\Gamma_2 \neq \Gamma_1$, except that the angles of the rays separating growing from decaying motions change.

The $\Theta < 0$ phase surface is foliated by closed orbits surrounding the singularity $\mathscr{S}_3$. The $\Theta > 0$ has one equilibrium $\mathscr{E}_3$, from which emerge a pair of homoclinic orbits, each encircling singularity $\mathscr{S}_1$ or $\mathscr{S}_2$.

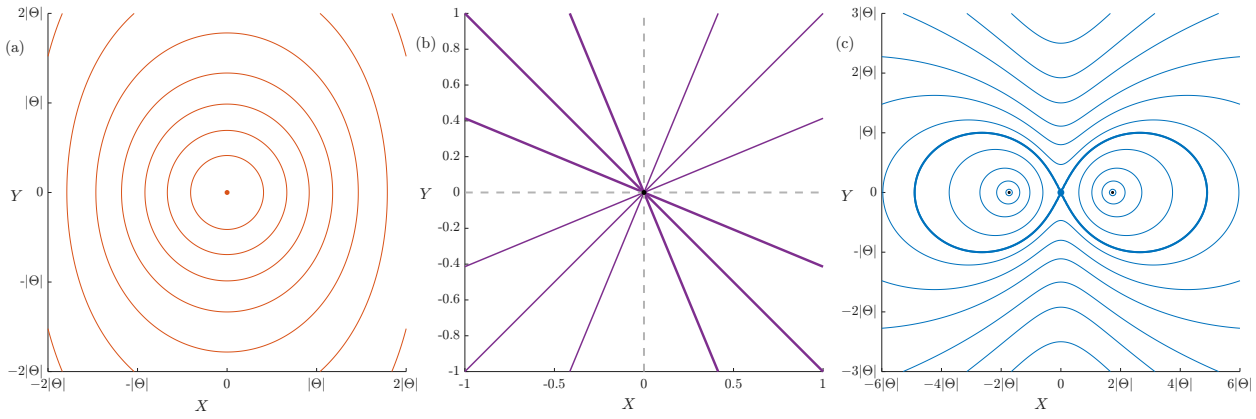

FIGURE 4.6. The XY phase planes in case **e** with $\Gamma_3 = \frac{-1}{3}$. The trajectories in the $\Theta = 0$ case are rays through the origin and correspond to triangles that shrink to zero in finite forward time (quadrants one and three), finite backward time (quadrants two and four), or do not change size (the X- and Y-axes).

Point d: $\Gamma_3 = \frac{-1}{2}$. As Γ_3 decreases past the value $\frac{-1}{3}$, the four equilibria return from infinity and appear on the phase surfaces for $\Theta < 0$ with their stability types exchanged: the two triangular configurations $\mathscr{E}^{\pm}_{\text{tri}}$ are saddles, and the collinear configurations $\mathscr{E}_1$ and $\mathscr{E}_2$ are centers. The saddles are connected by two pairs of heteroclinic orbits: one pair surrounds the singularity $\mathscr{S}_3$ at the origin and a second, longer pair, each of which makes a wide excursion around a collinear equilibrium $\mathscr{E}_1$ or $\mathscr{E}_2$. All orbits on the surface $\Theta = 0$ are closed. The $\Theta > 0$ phase surface is unchanged from the previous plot. Understanding the $\Theta < 0$ takes

some care. Two of the heteroclinic curves connecting the triangular equilibria take excursions that include them, the left panel of Fig. 4.7 includes a very large region of the phase surface. At this scale, the equilibria, singularities, and smaller heteroclinic curves are not visible. As such, Fig. 4.8 contains a closeup of this figure showing these features.

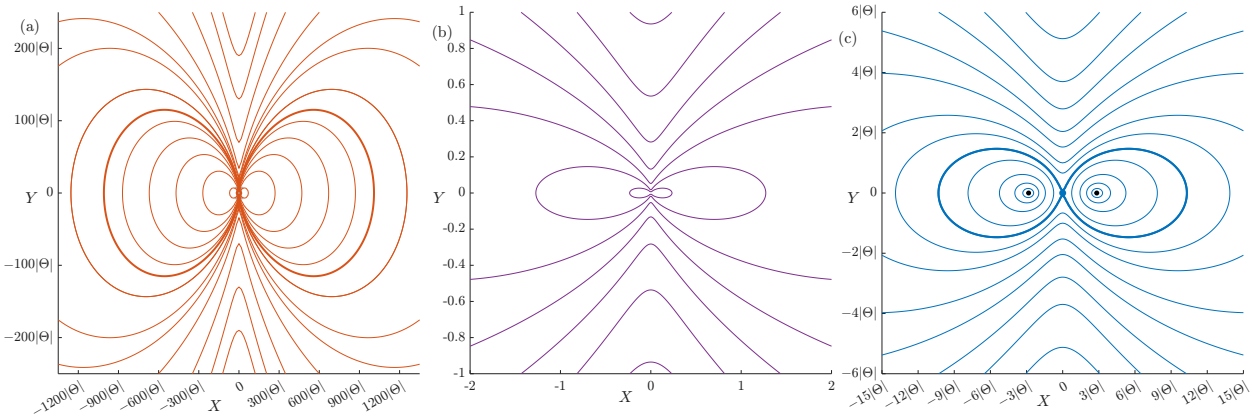

FIGURE 4.7. The XY phase planes of system in case **d** with $\Gamma_3 = \frac{-1}{2}$. The two equilibria $\mathscr{E}_1$ and $\mathscr{E}_2$ have moved to the $\Theta < 0$ surfaces and become centers. The two equilibria $\mathscr{E}_{\text{tri}}^{\pm}$ have returned to the $\Theta < 0$ surfaces but have become centers. A thicker curve denotes the larger loops of the heteroclinic orbits, but the smaller segments are invisible at this magnification. Therefore, we show a closeup of the left image in Fig. 4.8.

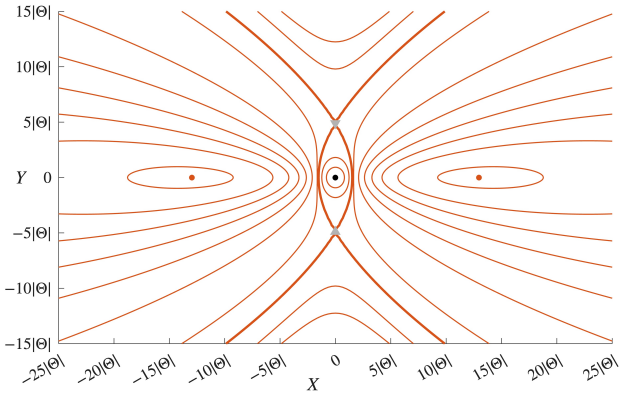

FIGURE 4.8. A closeup of the $\Theta < 0$ phase surface showing the singularities and equilibria as well as the smaller components of the heteroclinic curves.

Point c: $\Gamma_3 = -1$. As Γ_3 approaches -1, the collinear equilibria $\mathscr{E}_1$ and $\mathscr{E}_2$ diverge to $X = \pm\infty$, as do the singularities $\mathscr{S}_{13}$ and $\mathscr{S}_{23}$. At $\Gamma_3 = -1$, they all cease to exist. This is because at $\Gamma_3 = -1$, vortex 3 may form a dipole with either of the other two vortices. Since the total circulation of the two vortices forming the dipole vanishes, their joint center of vorticity sits at infinity.

This is the second case in which unbounded orbits exist. They correspond to orbits in which a vortex dipole scatters off a third, initially stationary vortex. In [1], we used the phase surface plots in Fig. 4.9 to derive a simplified explanation of this scattering phenomenon. In that paper, we analyze the scattering dynamics when the third vortex has arbitrary circulation. This occurs for circulations along either of the dashed lines through point **c** in Fig. 3.1.

For this value of Γ_3, when $\Theta = 0$, the three vortices must always lie a the corners of a right triangle, a fact observed by Gröbli [13]. As such, the area formed by this triangle cannot vanish and $Y \neq 0$. Hence the X-axis is singular on this phase surface, as represented by the gray line in the center panel of Fig. 4.9.

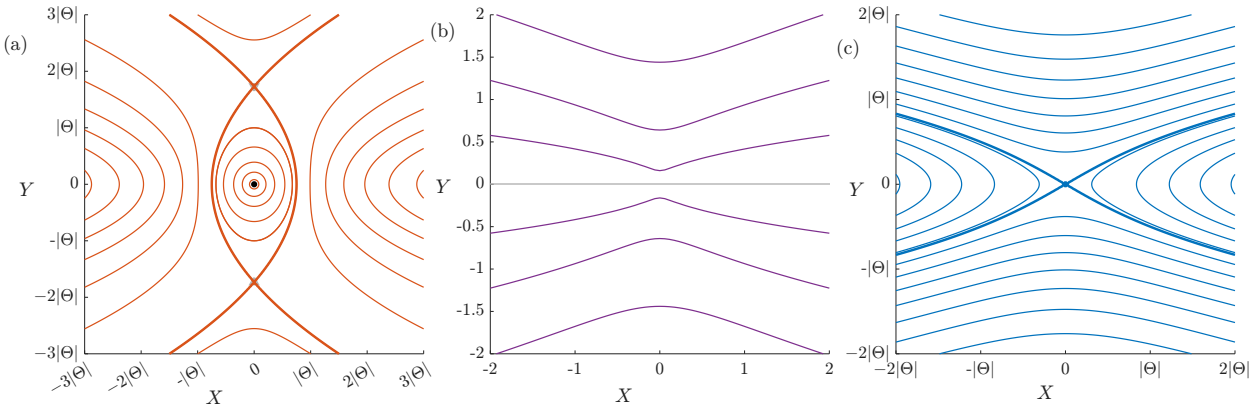

FIGURE 4.9. The XY phase planes for case **c** with $\Gamma_3 = -1$. (a) The case $\Theta < 0$ with singularity X_{12} at the origin and triangular configurations (X,Y,Z) at the intersections of the thick curves. (b) The case $\Theta = 0$. The gray line $Y = 0$ is singular. (c) The case $\Theta > 0$ with collinear equilibrium at the origin.

Point b: $\Gamma_3 = \frac{-3}{2}$**.** The phase surface for point **b** with $\Gamma_3 = \frac{-3}{2}$, shown in Fig. 4.10 looks almost unchanged from the surface at point **d**, but there is one crucial difference. The equilibria and singularities that diverged to infinity at point **c** have returned from infinity, only now the two singularities $\mathscr{S}_{13}$ and $\mathscr{S}_{23}$ lie on the $\Theta < 0$ surface and the collinear equilibria $\mathscr{E}_1$ and $\mathscr{E}_2$ lie on the $\Theta > 0$ surface.

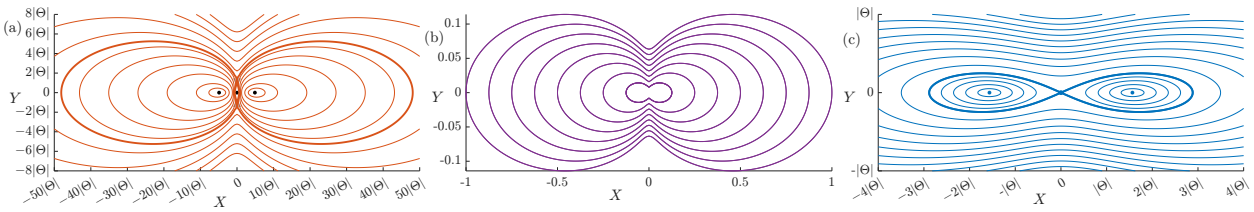

FIGURE 4.10. The XY phase planes of system in case **b** with $\Gamma_3 = \frac{-3}{2}$.

Point a: $\Gamma_3 = \frac{-17}{3}$**.** Finally, as Γ_3 is further decreased below $\Gamma_3 = \frac{-5}{3}$, where deltoid has its cusp in Fig. 3.1 to point **a**, the three collinear equilibria collide in a pitchfork bifurcation. Only $\mathscr{E}_3$ survives, changing from an unstable saddle to a stable center.

5. VANISHING TOTAL CIRCULATION

The last step of the Jacobi reduction can not be applied if the total circulation vanishes, and we need to use an alternate procedure. we may always label the particle so that the sequence of transformations works at each step except the last. Therefore, we need an alternative to the reduction described by Eqs. (2.16) that applies in the dipole case when $\Gamma_1 + \Gamma_2 = 0$. Ohsawa has noted the need for a different reduction method when the total circulation vanishes [27].

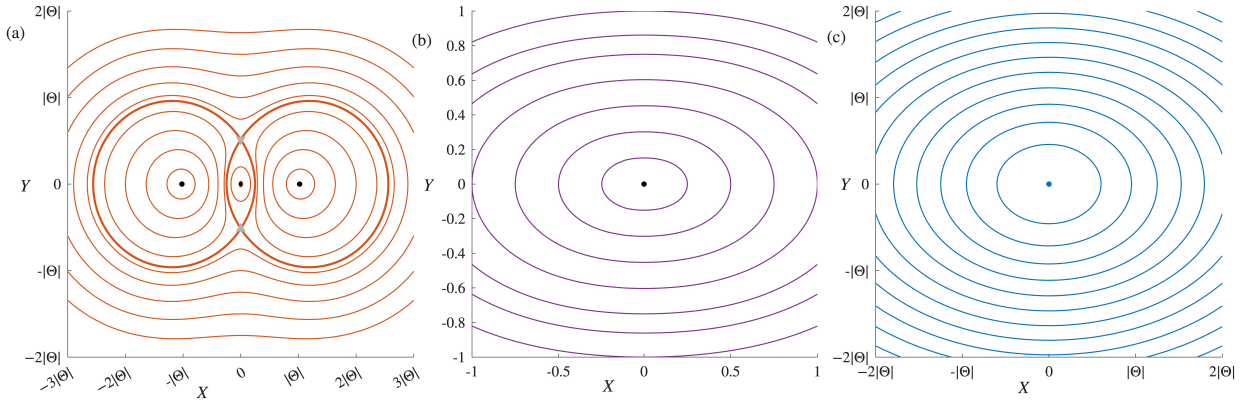

FIGURE 4.11. The XY phase planes in case **a** with $\alpha = \frac{-17}{3}$.

5.1. **The reduction method.** Consider first a system with two vortices of circulations $\pm 2\pi\Gamma_1$. Consulting Fig. 2.1, we define two position coordinates Q_j and momentum vectors P_j

$$\begin{aligned} Q_1 &= \frac{x_1+x_2}{2}, \quad Q_2 = \frac{y_1+y_2}{2}, \\ P_1 &= y_1 - y_2, \quad\quad P_2 = -x_1 + x_2. \end{aligned} \tag{5.1}$$

The Hamiltonian becomes

$$H = \frac{\Gamma_1^2}{2}\log\left(P_1^2+P_2^2\right).$$

The Poisson bracket, and thus the evolution equations, maintain the dependence on the circulations' magnitudes but not their signs.

$$\frac{\mathrm{d}Q_j}{\mathrm{d}t} = \frac{1}{\Gamma_1}\frac{\partial H}{\partial P_j}, \frac{\mathrm{d}P_j}{\mathrm{d}t} = \frac{-1}{\Gamma_1}\frac{\partial H}{\partial Q_j}, \quad \text{for} \quad j = 1,2.$$

The momenta are conserved since H is Q_j-independent, and the particles move in a straight line at constant velocity

$$\frac{\mathrm{d}}{\mathrm{d}t}(Q_1,Q_2) = \frac{\Gamma_1}{P_1^2+P_2^2}\cdot(P_1,P_2)\,.$$

By choosing the orientation of the reference frame, we may set one component of the momentum, say P_2, to zero.

This is somewhat different than the Hamiltonian formulation (2.2), in which the x and y coordinates play the roles of position in momentum. Here, we have returned to the more standard case in which Q variables represent positions and P variables momenta.

Returning to the three-vortex problem, assume that $\gamma_1 = 0$, or, equivalently, $\Gamma_3 = -\Gamma_1 - \Gamma_2$. Ordering the vortex labels so that $\Gamma_1 + \Gamma_2 \neq 0$, we may perform the first step of the Jacobi reduction as before, arriving at system (2.16). However, the second recursive application of the Jacobi coordinate reduction leading to Eq. (2.17) is no longer possible. We may instead apply the transformation (5.1) to the coordinates $\tilde{z}_2$ and $\tilde{z}_3$. Without loss of generality, we may take $P_2 = 0$. If $P_3 \neq 0$, we may, by scaling, set $P_3 = 1$ without loss of generality. Letting $Q_1 = X$ and $P_1 = Y$ and ignoring additive constants, this yields a Hamiltonian

$$\begin{aligned} H = &-\frac{\Gamma_1\Gamma_2}{2}\log\left(X^2+Y^2\right) + \frac{(\Gamma_1+\Gamma_2)\Gamma_1}{2}\log\left(\left(\Gamma_1+\Gamma_2(X-1)\right)^2+\Gamma_2^2Y^2\right) \\ &+\frac{(\Gamma_1+\Gamma_2)\Gamma_2}{2}\log\left(\left(\Gamma_2+\Gamma_1(X+1)\right)^2+\Gamma_1^2Y^2\right). \end{aligned} \tag{5.2}$$

The three singularities are at $Y = 0$ and

$$X_{12} = 0, \quad X_{13} = 1 - \frac{\Gamma_1}{\Gamma_2}, \quad X_{23} = -1 - \frac{\Gamma_2}{\Gamma_1}.$$

Rott and Aref derived this system separately by different methods which were much more involved than the present derivation [3, 29]. Behring derived the equivalent system when $\Gamma_1 = \Gamma_2$ [6].

When $P_2 = P_3 = 0$, this reduces further to

$$H = \frac{\Gamma_1^2 + \Gamma_2\Gamma_1 + \Gamma_2^2}{2} \log\left(X^2 + Y^2\right), \tag{5.3}$$

again ignoring an additive constant.

5.2. **Relative equilibria and global phase portrait.** The system described by Hamiltonian (5.2) has equilateral relative equilibria at

$$\mathscr{E}_{\text{tri}}^{\pm} = \left(\frac{\Gamma_2^2 - \Gamma_1^2}{2\left(\Gamma_1^2 + \Gamma_2\Gamma_1 + \Gamma_2^2\right)}, \pm \frac{\sqrt{3}\left(\Gamma_1 + \Gamma_2\right)^2}{2\left(\Gamma_1^2 + \Gamma_2\Gamma_1 + \Gamma_2^2\right)} \right), \tag{5.4}$$

A standard computation shows these are saddles connected pairwise by heteroclinic orbits. One such phase plane is shown in Fig. 5.1.

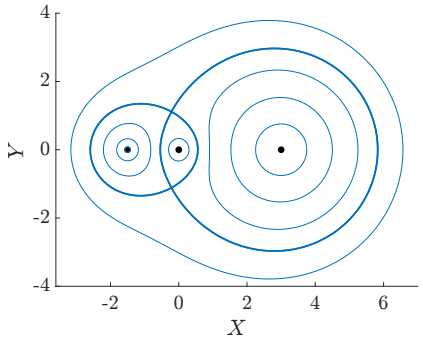

FIGURE 5.1. A phase plane with vanishing total circulation, $(\Gamma_1, \Gamma_2, \Gamma_3) = (2, 1, -3)$.

When $\Gamma_1 = \Gamma_2$, the formula simplifies significantly, but there are no bifurcations. When $P_2 = 0$, the dynamics of Hamiltonian (5.3) has a lone singularity at the origin corresponding to a triple collision.

6. CONCLUSION

We have combined Ohsawa's geometric reduction with the method of Jacobi coordinates to derive a reduced set of evolution equations for the motion of three vortices in the plane. Compared with the trilinear formulation of the equations dating back to the works of Gröbli, Synge, Aref, and others [2, 13, 31], this new set of equations is easy to work with, since the reduction introduces neither singularities into the equations nor artificial boundaries into the phase plane. Using this formulation, we rederive, in a highly simplified form, earlier results found separately by Conte and Aref enumerating and classifying the stability of the system's relative equilibria [4, 10] and extending this to draw the full phase-plane dynamics. The reduction shows that the dynamics occurs on a quadric surface in three-dimensional space. Previously derived reduced systems are singular precisely at folds on the two-dimensional phase surface.

The trilinear formulation has also been used to study two other integrable cases of vortex motion: the motion of three vortices on a sphere [5, 17]. We aim to extend the analysis presented here to those more complicated systems of equations.

APPENDIX A. THE RESULTANT, THE DISCRIMINANT, AND DIXON'S RESULTANT

Aref gives an excellent introduction to the resultant and discriminant and applies it to this problem in Ref. [4]. We summarize the main ideas here and discuss Dixon's resultant, which applies to larger systems of equations.

The resultant. The resultant must vanish for two polynomials $a(x)$ and $b(x)$ to have a common root. Consider, for example, the case that $a(x) = a_2x^2 + a_1x + a_0$ and $b(x) = b_3x^3 + b_2x^2 + b_1x + b_0$. Augment the system

$$a(x) = 0, \quad b(x) = 0$$

with the redundant equations

$$x^2a(x) = 0, \quad xa(x) = 0, \quad \text{and} \quad xb(x) = 0.$$

These may be arranged into a linear system

$$\begin{bmatrix} a_2 & a_1 & a_0 & 0 & 0 \\ 0 & a_2 & a_1 & a_0 & 0 \\ 0 & 0 & a_2 & a_1 & a_0 \\ b_3 & b_2 & b_1 & b_0 & 0 \\ 0 & b_3 & b_2 & b_1 & b_0 \end{bmatrix} \begin{bmatrix} x^4 \\ x^3 \\ x^2 \\ x^1 \\ x^0 \end{bmatrix} = \begin{bmatrix} 0 \\ 0 \\ 0 \\ 0 \\ 0 \end{bmatrix}. \tag{A.1}$$

The matrix in this equation is called the Sylvester matrix, and a necessary condition for system (A.1) to have a solution is the vanishing of its determinant, which is known as the resultant of the two polynomials $\text{res}\,(p,q;x)$. The above construction generalizes straightforwardly to polynomials of arbitrary degree. The dimension of the Sylvester matrix is $\deg a + \deg b$, so the size and complexity of the resultant expression grows rapidly with the degrees of the two polynomials. Several equivalent definitions exist, and multiplying out the determinant is not an efficient algorithm to calculate it. The Mathematica command `Resultant` computes it.

The resultant is often used to find the roots of a system of two polynomials in two variables $p(x,y)$ and $q(x,y)$. Treating each as a polynomial in y with x-dependent coefficients, the resultant eliminates y, returning a single higher-order polynomial for x, which may be treated by standard methods. The degree of this polynomial then gives the number of (possibly complex-valued) roots.

The discriminant. We are interested in how the number of roots of a polynomial $p(x,\mu)$ change as a parameter μ varies, i.e., in the bifurcations of the roots of p. At such values $p(x,\mu)$ and $p'(x,\mu)$ vanish simultaneously. The *discriminant* of p is proportional to the resultant of p and p'. It generalizes the $b^2 - 4ac$ term in the quadratic formula whose vanishing indicates a double root of the quadratic equation. Mathematica has a `Discriminant` function to compute it.

Dixon's resultant. As the resultant finds the condition for two polynomials in one variable to have a common root. Dixon's resultant generalizes this to find conditions that $n+1$ equations in n variables have a common root [12]. An algorithm to compute it is due to Kapur et al. [16] and was implemented for Mathematica by Lichtblau [20]. We attempted to use the Dixon resultant to calculate the function in Eq. (3.10), which vanishes at the circulation values where the stability of the collinear relative equilibria change. The resulting matrices were so large that Mathematica failed to return an answer in a reasonable time. Instead, we used the following procedure, which is less sophisticated but worked to find the conditions under which three functions $a(x,y)$, $b(x,y)$, and $c(x,y)$ have a common root. First eliminate y by computing $A(x) = \text{res}\,(a,b;y)$ and $B(x) = \text{res}\,(b,c;y)$, and then eliminate x by computing the third resultant $\text{res}\,(A,B;x)$.

Appendix B. Trilinear coordinates for the plane

To define trilinear coordinates, we define three points equispaced on the unit circle,

$$(x_1,y_1)=(0,1),\quad (x_2,y_2)=\left(\frac{-\sqrt{3}}{2},\frac{-1}{2}\right),\quad (x_3,y_3)=\left(\frac{\sqrt{3}}{2},\frac{-1}{2}\right).$$

Then, the coordinates (x,y), defined by the affine combination

$$x=\eta_1x_1+\eta_2x_2+\eta_3x_3,\quad y=\eta_1y_1+\eta_2y_2+\eta_3y_3,$$

where the weights η_j satisfy Eq. (3.2), give the standard cartesian parameterization of $\mathbb{R}^2$.

Acknowledgments

The authors gratefully acknowledge support from the NSF under award DMS-2206016. They thank Tomoki Ohsawa for helpful discussions and Jared Bronski for pointing out (correctly!) that the curve describing bifurcations of collinear orbits might be Steiner's deltoid.

References

[1] A. Anurag, R. H. Goodman, and E. K. O'Grady. A new canonical reduction of three-vortex motion and its application to vortex-dipole scattering. *Phys. Fluids*, 36:067110, 2024.

[2] H. Aref. Motion of three vortices. *Phys. Fluids*, 22:393, 1979.

[3] H. Aref. Three-vortex motion with zero total circulation: Addendum. *Z. Angew. Math. Phys.*, 40:495–500, 1989.

[4] H. Aref. Stability of relative equilibria of three vortices. *Phys. Fluids*, 21:094101, 2009.

[5] H. Aref and M. A. Stremler. Four-vortex motion with zero total circulation and impulse. *Phys. Fluids*, 11:3704–3715, 1999.

[6] B. M. Behring. *Dances and escape of the vortex quartet*. PhD thesis, New Jersey Institute of Technology, 2020.

[7] A. V. Bolsinov, A. V. Borisov, and I. S. Mamaev. Lie algebras in vortex dynamics and celestial mechanics-IV. *Regul. Chaotic Dyn.*, 4:23–50, 1999.

[8] A. V. Borisov and A. E. Pavlov. Dynamics and statics of vortices on a plane and a sphere—I. *Regul. Chaotic. Dyn.*, 3:28–38, 1998.

[9] A. J. Chorin and J. E. Marsden. *A Mathematical Introduction to Fluid Mechanics*, volume 4 of *Texts in Applied Mathematics*. Springer-Verlag, 3rd edition, 1993.

[10] R. Conte. Étude d'écoulements bidimensionnels tourbillonnaires: Mouvement de trois ou quatre tourbillons ponctuels et de nappes tourbillonnaires. Thèse d'Etat,Université Paris VI, 1979.

[11] R. Conte and L. de Seze. Exact solution of the planar motion of three arbitrary point vortices. *Mod. Phys. Lett. B*, 29:1530017, 2015.

[12] A. L. Dixon. The eliminant of three quantics in two independent variables. *Proc. London Math. Soc.*, s2-7:49–69, 1909.

[13] W. Gröbli. *Spezielle probleme Über die Bewegung geradliniger paralleler Wirbelfäden*. PhD thesis, Georg-August-Universität Göttingen, 1877.

[14] A. Hernández-Garduño. Three-point vortex dynamics as a lie-poisson system, 2019.

[15] A. Hernández-Garduño and B. N. Shashikanth. Reconstruction phases in the planar three- and four-vortex problems. *Nonlinearity*, 31:783–814, 2018.

[16] D. Kapur, T. Saxena, and L. Yang. Algebraic and geometric reasoning using Dixon resultants. In *Proceedings of the International Symposium on Symbolic and Algebraic Computation*, ISSAC '94, pages 99–107, New York, NY, USA, 1994. Association for Computing Machinery.

[17] R. Kidambi and P. K. Newton. Motion of three point vortices on a sphere. *Phys. D*, 116:143–175, 1998.

[18] G. Kirchhoff. *Vorlesungen über mathematische Physik: Mechanik*, volume 1 of *Vorlesungen über mathematische Physik*. Teubner, Leipzig, 1876.
[19] V. S. Krishnamurthy, H. Aref, and M. A. Stremler. Evolving geometry of a vortex triangle. *Phys. Rev. Fluids*, 3:024702, 2018.
[20] D. Lichtblau. Wolfram Repository Dixon Resultant v1.1. https://resources.wolframcloud.com/FunctionRepository/resources/DixonResultant/, 2023.
[21] Q. Luo, Y. Chen, and Q. Liu. Global phase diagrams of three point vortices. *Int. J. Bifurcation Chaos*, 32:2250025, 2022.
[22] J. E. Marsden and T. S. Ratiu. *Introduction to Mechanics and Symmetry*. Springer, 1999.
[23] R. Montgomery. The three-body problem and the shape sphere. *Am. Math. Mon.*, 122:299–321, 2015.
[24] P. K. Newton. *The N-Vortex Problem, Analytical Techniques*. Springer, 2001.
[25] E. A. Novikov. Dynamics and statistics of a system of vortices. *Sov. Phys. JETP*, 41:937–943, 1975.
[26] T. Ohsawa. Symplectic reduction and the Lie–Poisson shape dynamics of N point vortices on the plane. *Nonlinearity*, 32:3820–3842, 2019.
[27] T. Ohsawa. Nonlinear Stability of Relative Equilibria in Planar N-Vortex Problem. *arXiv*, math-ph 2406.12144, 2024.
[28] T. Ohsawa. Relative Dynamics of Vortices in Confined Bose–Einstein Condensates. *arXiv*, math-ph 2409.07657, 2024.
[29] N. Rott. Three-vortex motion with zero total circulation. *Z. Angew. Math. Phys.*, 40:473 – 494, 1989.
[30] M. A. Stremler. Something old, something new: Three point vortices on the plane. *Regul. Chaotic. Dyn.*, 26:482–504, 2021.
[31] J. L. Synge. On the motion of three vortices. *Can. J. Math.*, 1:257–270, 1949.
[32] J. Tavantzis and L. Ting. The dynamics of three vortices revisited. *Phys. Fluids*, 31:1392, 1988.
[33] H. von Helmholtz. Über Integrale der hydrodynamischen Gleichungen, welche den Wirbelbewegungen entsprechen. *J. Reine Angew. Math*, 55:25–55, 1858.

Email address: aa2894@njit.edu

DEPARTMENT OF MATHEMATICAL SCIENCES, NEW JERSEY INSTITUTE OF TECHNOLOGY, 323 MARTIN LUTHER KING BLVD., NEWARK NJ, 07102

Email address: goodman@njit.edu

DEPARTMENT OF MATHEMATICAL SCIENCES, NEW JERSEY INSTITUTE OF TECHNOLOGY, 323 MARTIN LUTHER KING BLVD., NEWARK NJ, 07102